Late Permian continental sediments in the SE Iberian Ranges, eastern Spain: Petrological and mineralogical characteristics and palaeoenvironmental significance

M. Isabel Benito [a,*], Raúl de la Horra [a], José F. Barrenechea [b], José López-Gómez [a], Magdalena Rodas [b], Jacinto Alonso-Azcárate [c], Alfredo Arche [a], Javier Luque [b]

[a] *Departamento de Estratigrafía, Instituto de Geología Económica, Facultad de Ciencias Geológicas, Universidad Complutense de Madrid, 28040-Madrid, Spain*

[b] *Departamento de Cristalografía y Mineralogía, Facultad de Ciencias Geológicas, Universidad Complutense de Madrid, 28040-Madrid, Spain*

[c] *Facultad de Ciencias del Medio Ambiente, Fábrica de Armas, Universidad de Castilla-La Mancha, 45071-Toledo, Spain*

Abstract

A detailed mineralogical and petrological study and the analysis of paleosol profiles in continental alluvial sediments of the Late Permian in the SE Iberian Ranges (Spain) allow us to infer the significant environmental changes that occurred during this time period. Three parts have been distinguished in the Late Permian sediments (Alcotas Formation). The lower part includes abundant and well-preserved carbonate paleosol profiles and fine-grained sediments made up by quartz, feldspar, hematite and illite, with scarce kaolinite. The preservation of dolomicrite in some paleosols suggests that they originally developed as dolocretes in an arid to semi-arid climate with marked seasonality.

A change towards more humid and acid conditions can be deduced from the presence of siderite and goethite in paleosols in the middle part of the Alcotas Formation. Moreover, the presence of plant remains, coal beds and/or carbonaceous shales at the top of the middle part, and the lack of carbonate paleosols in the upper part of the formation would indicate a further step towards acid conditions. These conditions would increase until the Early Triassic, as indicated by the lack of carbonates and the presence of Sr-rich aluminium phosphate sulphates (APS minerals) at the base of the Triassic (Cañizar Formation), which clearly indicates extreme acid conditions during the Permian–Triassic transition of the study area.

Keywords: Late Permian; Acid conditions; Iberian Ranges; Continental sediments; Paleosols; APS minerals

1. Introduction

During the Permian–Triassic transition, dated at 251 Ma (Menning, 2001), the Earth experienced the most severe crisis in its history. Both marine and terrestrial life suffered this crisis and it is estimated that 93–95% of all marine species (Raup, 1979) and about 70% of all vertebrate families (Maxwell, 1992) disappeared, which is twice as many groups as at the end-Ordovician marine mass extinction and many more than during the end-Cretaceous event.

Although the Permian–Triassic transition mass extinction and its possible causes are receiving far more attention now than in past decades, there are still controversies about the origin of the interrelated processes that resulted in that crisis. Furthermore, Late Permian sediments below the Permian–Triassic Boundary (PTB) already show clear evidence of stepwise mass extinctions (Stanley and Yang, 1994; Wignall et al., 1998; Kozur, 1998; Jin et al., 2000; Benton, 2003), which could support the idea of linked causes.

Interpretations about this crisis are not equally clear in all the Late Permian rocks since those of marine origin show more paleontological evidence. As adequate correlation between rocks of marine and continental origin has not been established for the PTB, it is difficult to determine whether the terrestrial events were exactly contemporaneous with those in the oceans. Studies of the continental record are crucial for determining whether the mechanisms of the crisis and extinction are the same as those observed in the marine record. Although there is growing evidence that tetrapods and insects also suffered considerable extinction, and that plant assemblages provide additional evidence of severe disturbance (Erwin, 1996), the geochemical and mineralogical response to the crisis on land was probably different from the one recorded in marine sediments. Detailed geochemical and mineralogical analysis such as those of Holster and Magaritz (1992), Retallack (1999), Krull and Retallack (2000) and Beauchamp and Baud (2002) may produce the key for a better understanding of the Permian–Triassic transition from a global perspective.

This paper intends to contribute to the better understanding of the environmental changes by means of the mineralogical characterization of fine-grained sediments and paleosol profiles of the continental Late Permian rocks of the SE Iberian Ranges, eastern Spain. A detailed study of a series of selected sections in a very complete succession of rocks in this area allows us to identify the changing mineral composition across this transition. These variations are discussed in terms of palaeoenvironmental changes and they are related to the mineralogical assemblages described in other regions.

2. Geological setting

During Late Permian–Early Triassic Iberia was a microplate located in the eastern part of Pangea in equatorial latitudes (Ziegler, 1990; Ziegler and Stampfli, 2001). By this time the western propagation of the Neotethys and the strike–slip motion of the Pyrenean and Gibraltar fault zones produced an extensional regime in the microplate, resulting in the creation of several extensional basins: the Iberian, Catalan and Pyrenean basins (Fig. 1).

The data presented in this paper have been obtained from the Permian–Triassic transition rocks of the southern Iberian Range. The present-day Iberian Range is a linear structure of Tertiary origin in central-eastern Spain, created by tectonic inversion of the Mesozoic Iberian Basin during compressional tectonic events mainly during the Late Oligocene–Early Miocene (Muñoz and Casas, 1997), which resulted in thin-skinned deformation with the detachment level in the evaporitic Keuper facies. The long and complex extensional story of the Iberian Basin started during the Early Permian with the extensional collapse of the Hercynian belt and westward propagation of the Neotethys, and continued during the Late Permian and the Triassic (Sopeña et al., 1988; Ziegler, 1990; López-Gómez et al., 1998).

As in the rest of the basins of the Iberian microplate, the Upper Permian–Lower Triassic rocks in the Iberian Basin are represented by alluvial sediments that lasted until Anisian times, when the Tethys Sea reached (Landete Formation) the eastern Iberian microplate margin (Fig. 2) (Arche and López-Gómez, 1999). The PTB is not represented in the study area. It is probably located somewhere from the contact between the lower and upper conglomerate subunits of the Hoz de Gallo Formation to the lower

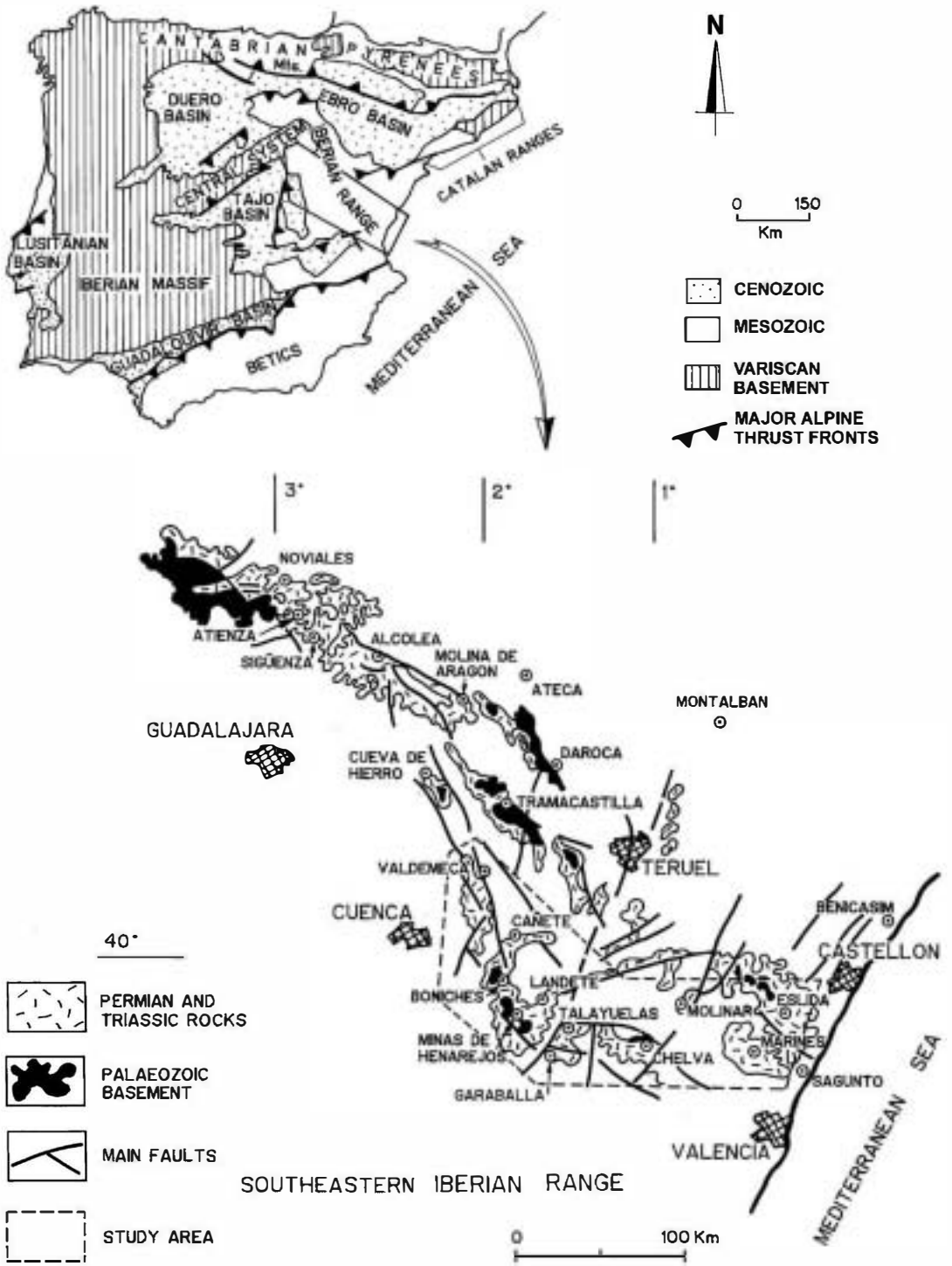

Fig. 1. Geographical and geological setting of the study area. Upper part shows the present-day main Cenozoic and Mesozoic basins and ranges and the major alpine thrust fronts.

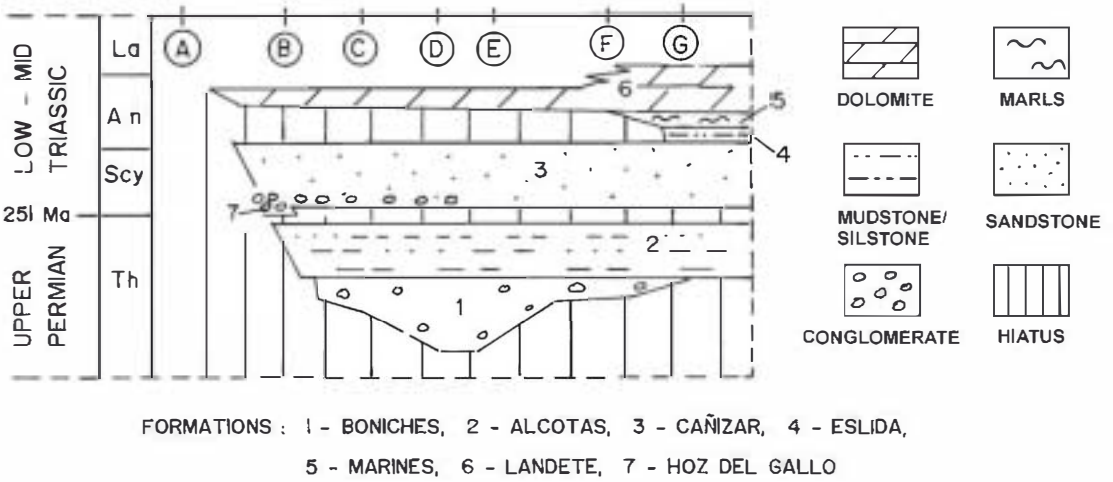

Fig. 2. Temporal and spatial range of the Permian–Triassic transition formations in the SE Iberian Ranges. Locations: A—North Valdemeca, B—South Valdemeca, C—Boniches, D—Henarejos, E—Talayuelas, F—Chelva, G—Molinar. See Fig. 1 for the location details.

part of the Cañizar Formation (Fig. 2) (López-Gómez et al., 2005). Sedimentation in the basin was controlled and isolated by different highs that crossed the basin until the end of the Permian when most of the highs were covered by alluvial sediments, very near to the Permian–Triassic transition.

The present study is based on a detailed analysis of the Alcotas Formation (Late Permian) and the base of the Cañizar Formation (Early Triassic) as exposed in six stratigraphic sections (Boniches, Landete, Talayuelas, Garaballa, Chelva and Chóvar–Eslida) from the study area (Fig. 3).

3. Analytical methods

For the mineralogical analysis 54 samples of red siltstones and mudstones were collected from the Alcotas and Cañizar Formations near the Permian–Triassic boundary (Fig. 3). The bulk sample mineralogy was obtained by X-ray diffraction (XRD) after grinding and homogenization of the samples to <53 μm. Random-oriented powders were examined on a Siemens Kristalloflex 810 diffractometer, using Cu-Kα at 40 kV and 40 mA, a step size of 0.03 (°2θ), and time per step of 1 s (scan rate of 1.8° 2θ/min). The clay mineral composition was determined on oriented aggregates of the <2 μm fraction obtained by sedimentation from an aqueous suspension onto glass slides. In some cases they were subjected to thermal treatment at 550 °C for 2 h and to solvation with ethylene glycol (EG). A slower scan rate (1.2° 2θ/min) was used between 2° and 13° 2θ in order to get better-defined peaks. Semi-quantitative analyses were performed following the method proposed by Schultz (1964).

In order to determine the intensity of the post-sedimentary processes that affected these samples, the full-width-half-maximum (FWHM) of the illite 10Δ reflection (the so-called Kübler index, KI) was measured on the diffractograms of the <2 μm material. Our data (y) were transformed to Crystallinity Index Standard (CIS) data (x) (Warr and Rice, 1994) by the formula: $y=0.869x+0.0022$. Therefore, KI values quoted in the following parts of this study have been converted to the CIS scale, in which the anchizone limits are 0.25–0.42°Δ2θ.

Petrographic microscopy was used for the study of thin sections to complement the mineralogical characterization of the samples. A more detailed study of the textural and morphological features of the minerals was performed on gold-coated chips of selected samples in a Jeol 6400 scanning electron microscope (SEM), equipped with an energy dispersive spectrometer (EDS).

Another 53 samples have been used for a petrographic and geochemical study of sedimentary and diagenetic features of paleosols, using standard petrographic techniques and cathodoluminescence, combined with an elemental analysis of carbonates. For

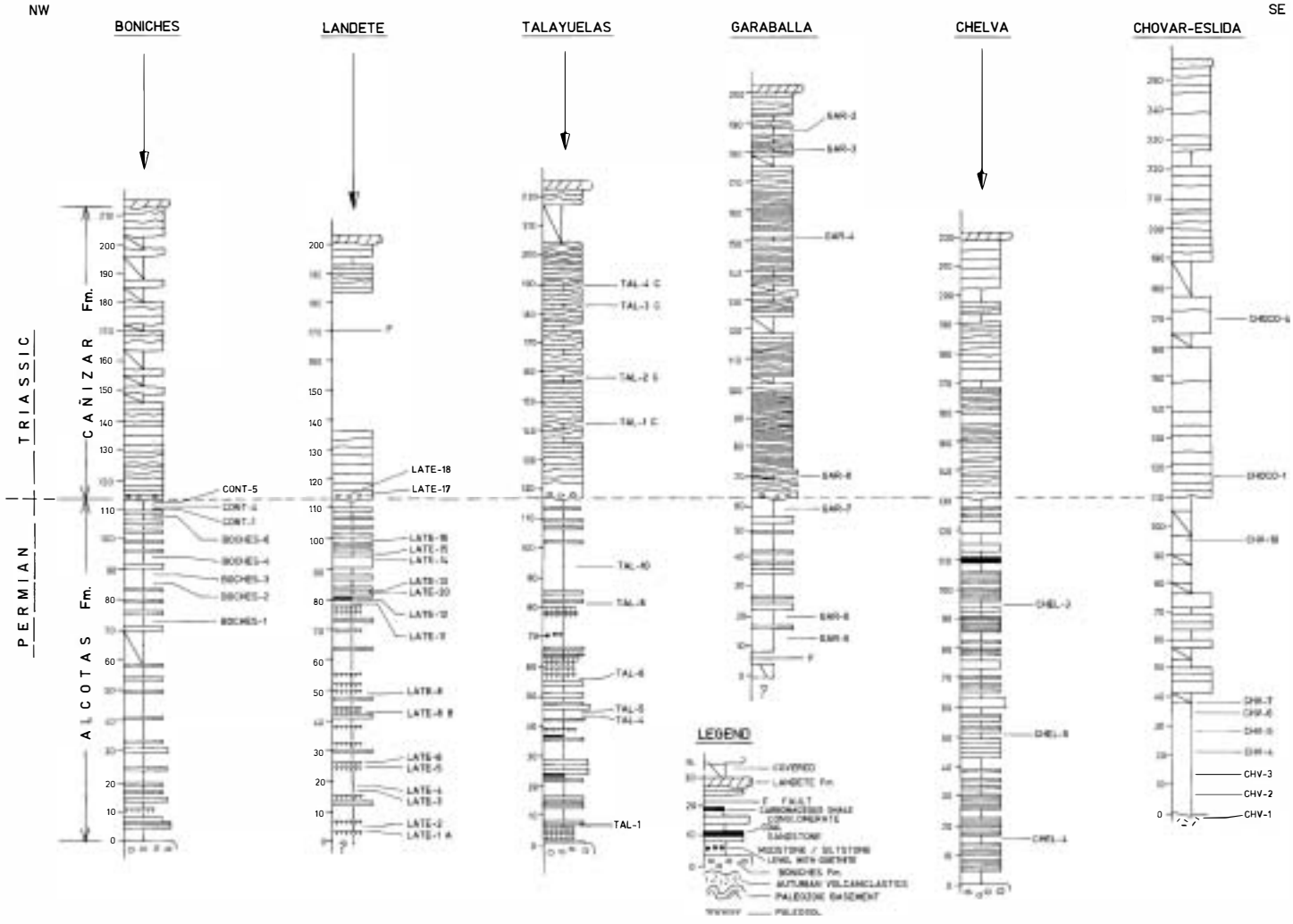

Fig. 3. Studied stratigraphical sections and location of the analysed samples. See Fig. 1 for the location of the sections.

each sample, a polished and uncovered thin section was prepared to 30 μm thickness for petrographic and geochemical analysis. Cathodoluminescent (CL) examination was carried out using a Technosyn® cold cathodoluminescent unit. Following examination with CL, all thin sections were stained with Alizarin Red S and potassium ferricyanide (Dickson, 1966). Elemental analysis for Ca, Mg, Sr, Mn, and Fe was performed on a JEOL JXA-8900 M WD/ED electron microprobe. All analyses were conducted with an accelerating voltage of 15 kV and a spot size of 5 μm. Detection limits were 100 ppm for Mg, 250 ppm for Sr, 200 ppm for Mn, and 250 ppm for Fe, and 140 ppm for Na.

4. The sediments

4.1. Depositional environments and age

Subsidence reconstructions (Arche and López-Gómez, 1996; Van Wees et al., 1998; Vargas, 2002) show that the Permian–Triassic extensional period can be subdivided into four distinct episodes bounded by angular unconformities or hiatuses. In this paper we only deal with sediments of the second and third episodes.

Early Permian: Represented by andesitic–basaltic volcanic rocks and dykes associated with lacustrine and fluvial sediments in isolated basins along the Iberian Range (Hernando et al., 1980; Doblas et al., 1993; Lago et al., 2001, in press).

Late Permian: Represented by red bed facies: conglomerate, sandstone and mudstone, usually known as "Saxonian facies" in the literature (Sopeña et al., 1988; Arche and López-Gómez, 1996). They were deposited in a broad asymmetric rift basin trending NW–SE. The episode ended with uplift and partial erosion.

Late Permian–Middle Triassic: Represented by the continental Buntsandstein facies and the shallow marine Röt and lower part of the Muschelkalk facies, deposited in a single rift basin (Sopeña et al., 1988; López-Gómez and Arche, 1993).

Middle Triassic–Early Jurassic: Represented by shallow marine carbonates and evaporites (Pérez-Arlucea and Sopeña, 1985; Ortí, 1987; Ortí et al., 1996; López-Gómez et al., 1998; Gómez and Goy, 1999).

The Late Permian sediments of the second episode are represented by the Boniches and Alcotas Formations (Fig. 2) (López-Gómez and Arche, 1993). This paper focuses on the Alcotas Formation and the base of the Cañizar Formation (Early Triassic).

The Alcotas Formation (López-Gómez and Arche, 1993), up to 170 m thick, consists of red to dark brown siltstone and mudstone layers and lenticular bodies of sandstone and locally conglomerate. The formation has been interpreted as deposits of seasonal braided rivers with high avulsion rate and extensive floodplains and shallow semi-permanent lakes that evolved towards the top to meandering rivers. Several pollen and spore assemblages of Late Permian (Thüringian) age have been found in the lower and middle parts of the Formation (Doubinger et al., 1990; Sopeña et al., 1995).

The third episode has a very complex vertical and horizontal facies distribution and it is constituted by the Hoz de Gallo Formation and the Cañizar Formation. The Hoz de Gallo Formation (Ramos, 1979; Ramos et al., 1986) only crops out in the NW area where it reaches up to 4 m thick (Fig. 2). It consists of quartzite conglomerate lying unconformably on the Alcotas Formation or on the Lower Paleozoic basement.

The Cañizar Formation (López-Gómez and Arche, 1993) is up to 170 m thick and consists of pink to white arkose with minor conglomerate and red mudstone layers. It has been subdivided into six subunits by means of regional erosion surfaces and interpreted as sandy braided river deposits. Paleocurrents point to the SE. It lies conformably on the Hoz de Gallo Formation or unconformably on the Alcotas Formation (Fig. 2).

4.2. Mineralogy of the fine-grained sediments

The results of the mineralogical characterization are presented in Table 1. Most of the samples analysed in the Alcotas and Cañizar Formations contain small angular to subrounded quartz and albite grains in a matrix composed of illite and hematite (Fig. 4a). Kaolinite has been detected in two samples from the Chelva section and small amounts of a chlorite/smectite mixed-layer are recognised in one sample from the Landete section by a reflection at 34.5 Å, which shifts to 36.1 Å upon ethylene-glycol solvation. Small proportions of strontium-rich aluminium phosphate sulphate minerals (goyazite/svanbergite) are detected on XRD traces of

Table 1
Variation in the mineralogical composition and Kübler index data (KI) of the samples collected along the studied cross-sections

Section	Sample	Qtz	Ill	Hem	Ab	Kln	Prl	APS	KI
Talayuelas	TAL4C	*	****		*				0.44
	TAL3C	*	****		*				0.52
	TAL2C	*	****						0.60
	TAL1C	*	****		*				0.61
	TAL10	**	****	*	*				n.d.
	TAL8	**	****	*	*				0.75
	TAL6	**	****	*	*				0.50
	TAL5	**	****	*	*				0.50
	TAL4	**	****		*				0.49
	TAL1	**	****	*	*				0.57
Boniches	CONT5	**	****	*	*				0.75
	CONT4	**	****	*	*				0.72
	CONT1	**	****	*	*				0.71
	BOCHES7	**	****	*	*				0.44
	BOCHES6	**	****	*	*				0.72
	BOCHES4	**	****	*	*				0.61
	BOCHES3	**	****	*	*				0.74
	BOCHES2	***	***	*	*				0.66
	BOCHES1	*	****	*	*				0.61
Chelva	CHEL3	**	****	*	*				0.57
	CHEL5	**	***	*	*	*			0.61
	CHEL4	**	****	*	*	*			0.58
Landete	LATE18	**	****	*	*				0.65
	LATE17	***	***						0.61
	LATE16	**	****	*	*				0.58
	LATE15	**	***	*	*				0.57
	LATE14	**	***	*	*				0.63
	LATE20	*	****		*				0.55
	LATE12	*	****		*				0.50
	LATE11	**	****		*				0.67
	LATE8	**	****	*	*				0.55
	LATE8B	***	***	*	*				0.61
	LATE6	***	**	*	*				0.70
	LATE5	**	****	*	*				0.71
	LATE4	**	****	*	*				0.72
	LATE3	**	****	*					0.55
	LATE2	**	****	*	*				0.67
	LATE1A	*	****	*	*				0.62
Garaballa	GAR2	*	****		*			*	0.65
	GAR3	*	****	*	*			*	0.65
	GAR4	*	****	*	*			*	0.57
	GAR8	*	****	*	*			*	0.51
	GAR7	*	****	*	*				0.65
	GAR6	*	****	*	*				0.53
	GAR5	*	****	*					0.62
Chóvar	CHOC04	**	***	*	*				0.36
	CHOC01	**	****	*	*				0.41
	CHV10	**	****	*	*				0.28
	CHV7	**	***	*	*		*		0.36
	CHV6	**	***	*	*		*		0.32
	CHV5	**	***	*	*		*		0.33
	CHV4	**	***	*	*		*		0.40
	CHV2	**	***	*	*		*		0.34
	CHV1	**	***	*	*				n.d.

Quartz (Qtz), hematite (Hem), albite (Ab) and goyazite/svanbergite (APS) contents were estimated from X-ray diffraction traces of unoriented mineral-aggregate samples, whereas illite (Ill), kaolinite (Kln) and pyrophyllite (Prl) contents were calculated from oriented aggregates of the <2-μm fraction. ****Major phase, (>50% in the semi-quantitative analyses), ***frequent phase (20 to 50%), **minor phase (10 to 20%), *accessory phase (<10%).

random-oriented powders from the Cañizar Formation in the Garaballa section (Fig. 3). Zircon, ilmenite and xenotime are present as accessory minerals within this section. The Kübler index data for the Boniches, Landete, Talayuelas, Garaballa and Chelva sections range between 0.44° and 0.75° Δ2θ and are clearly indicative of diagenetic conditions.

Samples from the Chóvar–Eslida section are red limolites with a similar mineralogical composition. However, the XRD analysis reveals the presence of pyrophyllite instead of kaolinite in six of the sam-

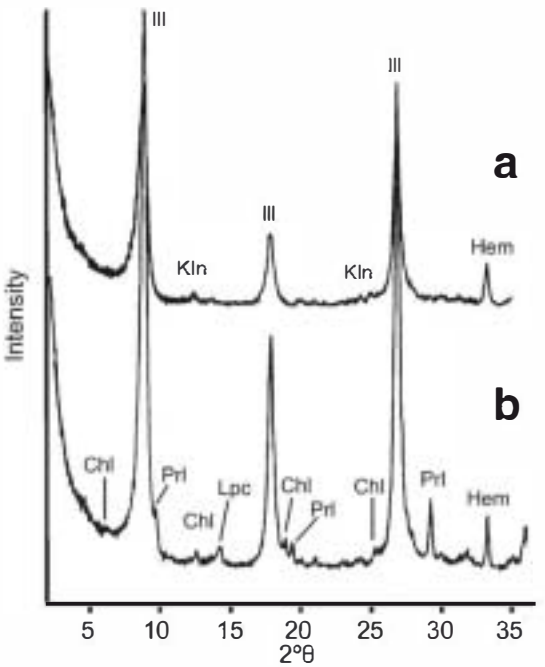

Fig. 4. XRD traces of oriented aggregates from (a) sample CHEL-4, representative of siltstones composed by illite and kaolinite and (b) sample CHV5, with a clay assemblage constituted by illite and pyrophyllite.

ples, together with traces of chlorite and lepidocrocite (Fig. 4b). This clay mineral assemblage, together with the lower KI data (0.28–0.41°Δ2θ), suggests that these samples were subjected to very low grade metamorphism.

The SEM study reveals that illite in most of the sections is found as roughly oriented platy crystals within the matrix (Fig. 5a) or as small fibres coating larger crystals (Fig. 5b). In samples from the Chóvar–Eslida section pyrophyllite commonly occurs as packets of slightly deformed crystals (Fig. 5c).

4.3. Paleosols description

Paleosols developed within the Alcotas Formation have been studied in detail in the western part of the study area, specifically in the Landete and Talayuelas stratigraphic sections (Figs. 3 and 6), where they are more abundant and best preserved. In the eastern part of the study area (Chelva and Chóvar–Eslida stratigraphic sections), subsidence was higher during the Late Permian (Vargas, 2002), and thus, paleosols are less abundant and poorly developed and no carbonate paleosols have been observed. Carbonate soil profiles with different stages of development have been recognized in the Landete and Talayuelas sections (Fig. 6). They correspond to the category of aridisols and vertisols proposed by Retallack (1993). In both sections the Alcotas Formation can be subdivided into three parts based on the presence or absence of paleosols, their type and stage of development and on the mineralogical composition (Fig. 6).

In the *lower part* paleosols are developed over alluvial sediments (Fig. 6) composed of red to brown sandstone, siltstone and mudstone. Pedogenic profiles commonly range between 25 cm and 1.5 m thick and they vary in their stage of development from stage I to stage III of Machette (1985). The dark red mudstone and/or siltstone contain scattered and small spherical to subspherical carbonate nodules (up to 22 mm in diameter) and root traces of about 13 cm long and 3–5 cm wide (Fig. 7a,b). Upwards in the profile, carbonate nodules are larger, up to 7 cm in diameter and, in some profiles, they form continuous layers of coalescing nodules that can be traced laterally at least 50 m (Fig. 7a). This calcareous horizon (15 to 55 cm thick) has a dark red colour or, in some cases, a mottled dark red to yellowish colour and typically displays a very well developed cracking structure composed of abundant angular and irregular cracks (up to 1 mm thick) (Fig. 7c). The horizon gradually passes upwards into a purple to dark red clayey horizon (Fig. 7a) with evidence of poorly preserved subangular blocky and platy peds. Maximum thickness of this upper horizon is 50 cm, with its top grading into the overlying red siltstone and mudstone or sharply truncated by bodies of sandstone. The mineralogy and texture of the original carbonate that precipitated in the calcareous horizons are not preserved in most of the paleosols because they are replaced by coarse and euhedral to subeuhedral dolomite and magnesite that precipitated during subsequent stages of diagenesis (Fig. 7c). The carbonate precursor has been only observed in the Talayuelas section, where it is constituted by dolomicrite that shows dark red luminescence and nodular texture (Fig. 7c).

The *middle part* of the Alcotas Formation consists of dark red mudstone with thin bodies of sandstone

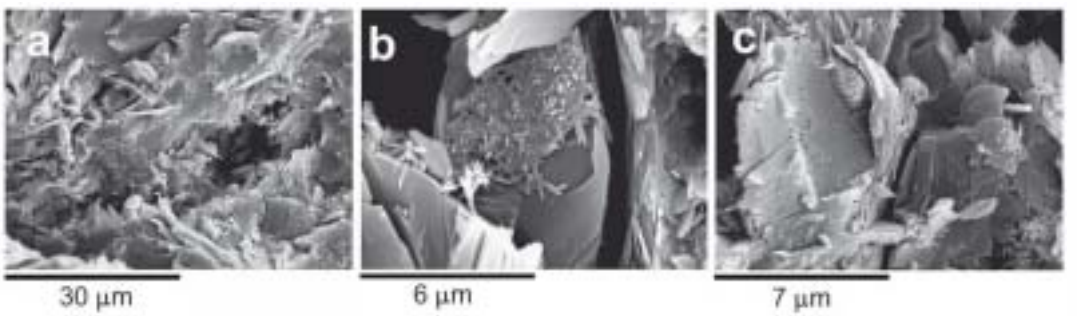

Fig. 5. SEM images of (a) roughly oriented illite (ill) platy crystals within the matrix; (b) small fibers of illite (ill) coating larger mica crystals; (c) stacks of slightly deformed crystals of pyrophyllite (prl).

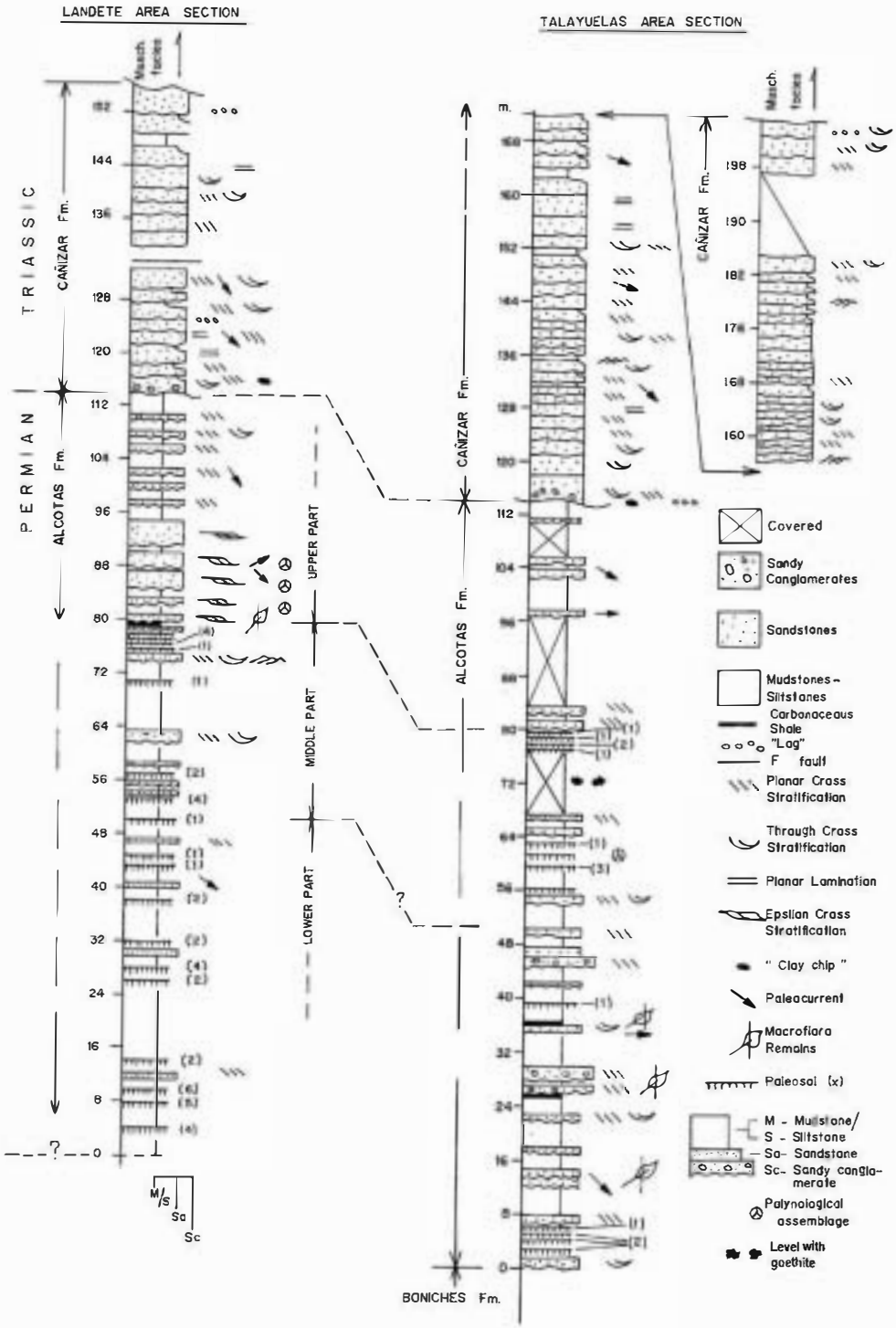

Fig. 6. Landete and Talayuelas sections in detail. Three parts (lower, middle and upper) have been differentiated in both sections by means of their mineralogical and petrological data and paleosols features. Figures in brackets indicate the number of studied samples in each paleosol.

interbedded (Fig. 6). In this part, paleosols vary from stage I to IV according to Machette's (1985) classification. Paleosol horizons formed in the middle part of the sequence are similar to those of the lower part of the Alcotas Formation, although they can be better developed (stage IV of Machette's classification) with a maximum thickness of 1 m (Fig. 7d). The calcareous horizon of these paleosols is composed of ferruginous mudstone that shows a lower part with coalescing carbonate nodules and an upper part, up to 20 cm thick, of solid brownish to yellowish carbonate with a sharp top and lateral continuity that can be traced for 100 m. It exhibits a weakly developed platy structure and abundant irregular cracks, associated with fossil root traces (Fig. 7c). The original mineralogy of the calcareous paleosol horizons developed in the middle part of the Alcotas Formation are not preserved because they were completely replaced by coarse dolomite and magnesite that precipitated during early stages of burial and obliterated the original pedogenic microstructure. In addition, these paleosols are affected by fractures that developed during late stages of burial. These fractures are filled by ankerite, barite and/or ferroan calcite.

The last two paleosols observed in the middle part of the Landete section contain two beds: the lower bed (up to 20 cm thick) is composed of mudstone or sandstone largely replaced by magnesite; the upper bed is a very dark layer, up to 7–10 cm thick, mainly composed of goethite, which preserves lenticular pseudomorphs of siderite, up to 7 mm long, that form aggregates (Fig. 7e–g). Only small relics of siderite ($Ca_{0.02}Mn_{0.12}Fe_{0.80}Mg_{0.06}CO_3$), less than 10 μm wide, are preserved in the pseudomorphs. Goethite may replace siderite crystals completely. More commonly, siderite pseudomorphs are constituted by goethite, calcite and ankerite (Fig. 7f, g). In this case, goethite precipitation mimics the external lenticular shape and the cleavage planes of the siderite precursor (Fig. 7g); the remaining porosity inside the pseudomorphs is filled by ankerite and ferroan calcite (Fig. 7g). Ankerite and calcite also fill fractures that postdate siderite and goethite precipitation (Fig. 7f).

In the Talayuelas section no paleosols containing siderite or siderite pseudomorphs have been recognized in the middle part of the sequence. However, accumulations of goethite precipitated around fossil plant fragments have been observed along some partially covered stratigraphic beds (Fig. 6).

The *upper part* of the Alcotas Formation contains dark orange to red mudstone and sandstone with no evidence of pedogenic carbonate precipitation (Fig. 6). The only preserved pedogenic features correspond to some diffuse, drab coloured (greenish-grey) haloes possibly developed around reduced root channels (Retallack, 1997). The base of the upper part of the Alcotas Formation in the Landete section is constituted by greenish to reddish lutites interbedded with carbonaceous shales (Fig. 7h). In addition, there are some thin and discontinuous layers, up to 1 cm thick, composed of siderite pseudomorphs, which are interbedded with the carbonaceous shales. Carbonaceous shales and/or coal beds similar to those of the Landete section have been observed in the upper part of the Alcotas Formation in the Chelva stratigraphic section (Fig. 3).

5. Discussion

Mineralogical studies may result in a key-tool for a better understanding of the palaeoenvironmental changes recorded during the poorly known Permian–Triassic transition in continental sediments. The SE Iberian Ranges show very good outcrops of this continental transition. A detailed mineralogical study from a combination of both fine-grained samples and soil profiles allows us to determine some of the main characteristics of the Late Permian general changes and their possible origin and consequences.

5.1. Mineralogical composition of the fine-grained sediments

The clay mineral assemblage of most of the Permian–Triassic sediments of the SE Iberian Ranges is formed predominantly by illite (with KI values that are characteristic of diagenesis) and minor amounts of kaolinite in some of the samples. However, the narrower 10 Å peaks measured in the Chóvar–Eslida section (0.28–0.41°Δ2θ) and the presence of pyrophyllite in some samples indicate that very low grade metamorphic conditions were attained in the area. The very low grade metamorphic clay assemblage is described for the first time within the SE Iberian Range. Preliminary data suggest that extensional tectonics and crustal thinning, combined with anomalously high subsidence rates (Van Wees et al.,

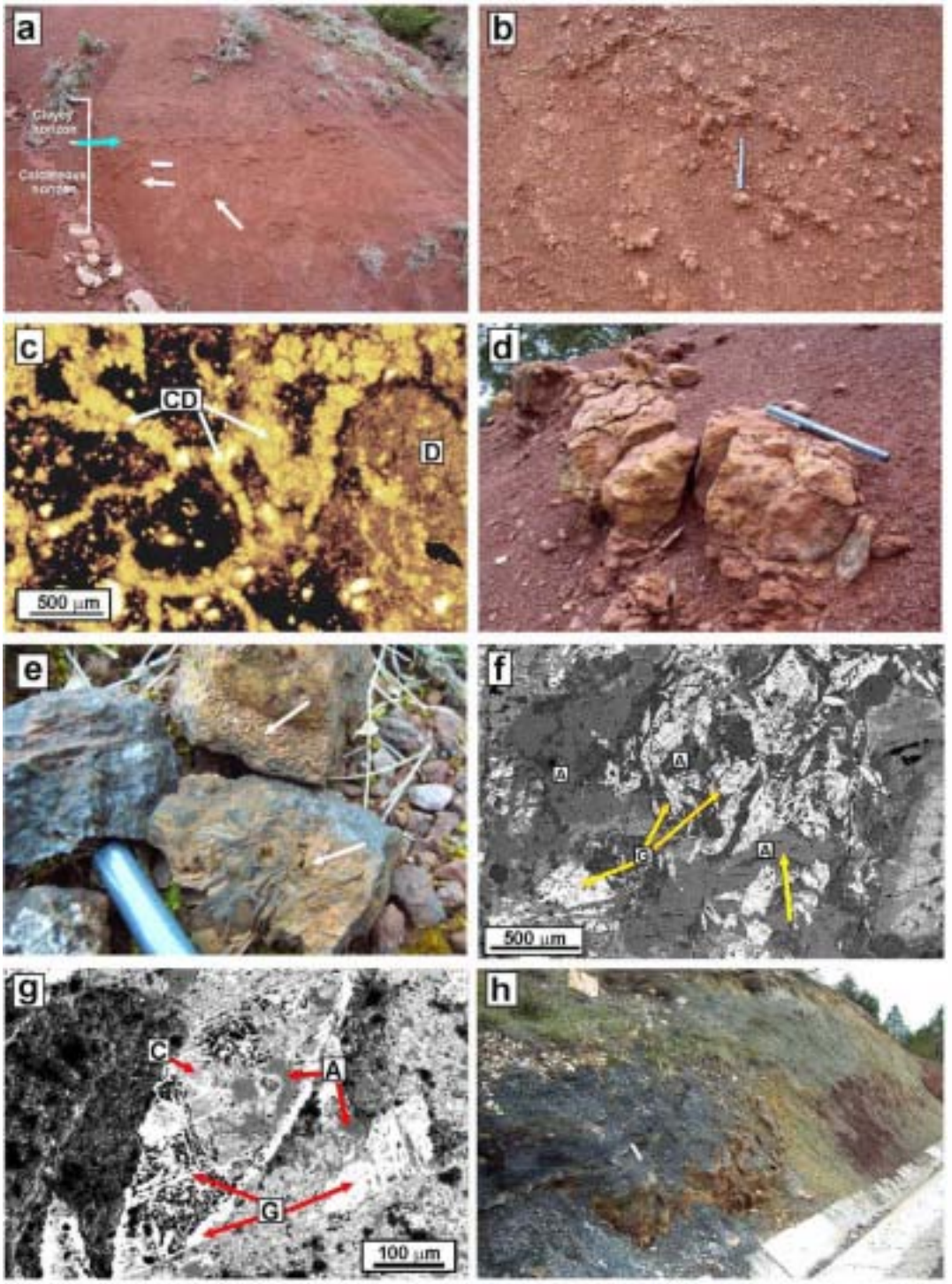
a
Clayey horizon
Calcareous horizon
b
c
CD
D
500 µm
d
e
f
A
A
C
A
500 µm
g
C
A
G
100 µm
h

1998; Vargas, 2002) are responsible for the development of the metamorphism. The extent of this anchimetamorphic event is currently under evaluation.

The presence of illitic clay as the predominant component of the fine-grained siliciclastic continental sediments is in agreement with previous studies of the Western European Permian–Triassic (Lucas, 1962; Fisher and Jeans, 1982; Lippmann and Berthold, 1992; Jeans et al., 1994; Ruiz Cruz, 1996; Marfil et al., 1996). Lindgreen and Surlyk (2000) found a more complex clay assemblage in the Permian–Triassic mudstone of East Greenland, with illite, chlorite, vermiculite and illite–smectite. The authors argued that discrete clay minerals in these rocks are largely detrital, derived from weathered Precambrian and Caledonian crystalline basement of Greenland.

In a study of Permian–Triassic rocks of the Alcaraz region (Spain), South Devon coast (U.K.), and deep wells in the Western Approches and Yorkshire, Jeans et al. (1994) conclude that much of the clay mica assemblage was formed originally in coeval deserts, and it was then eroded and deposited as detritus in adjacent areas. They claim that the ferric nature of the micas and the abundance of clay mica in the uppermost layers of soils from present-day arid regions support this assertion. Alternatively they suggest that much of the clay mica could have been wind transported from sources outside Europe. This wind-blown hypothesis was also considered in a previous work on the study area by Alonso-Azcárate et al. (1997) who suggested the Zechstein Basin (Poland) as the potential source area. Many of the arguments concerning the prevailing oxidizing conditions and clay mica development in soils of arid or semi-arid regions might apply to our samples.

5.2. Paleosol interpretation

The original carbonate mineralogy of most of the calcareous horizons developed in the lower part of the Alcotas Formation is uncertain because they are largely replaced by coarse dolomite and/or magnesite. These mineral assemblages are similar to those precipitated in the red beds of the Late Permian of Austria (Spötl and Burns, 1994). However, the preservation of dolomicrite in some horizons (Fig. 7c) suggests that they originally developed as dolocretes in an arid to semi-arid climate with marked seasonality (Wright and Tucker, 1991; Spötl and Wright, 1992; Alonso-Zarza, 2003).

It is not possible to determine the original mineralogy of carbonate paleosols of the middle part of the Alcotas Formation, because they are replaced by coarse magnesite and no relict of the carbonate precursor has been preserved. However, early diagenetic siderite has been observed in the dark bed developed at the top of these paleosols, just below and interbedded with the carbonaceous shales at the base of the upper part of the Landete section (Figs. 6 and 7h). Siderite has very low Mg and Ca and high Mn contents that are typical of siderites precipitated from meteoric-derived waters (Mozley, 1989). Siderite precipitation has been widely described as a very early diagenetic phase that commonly occurs in organic-rich marsh and swamp sediments deposited in floodplains and deltas (Coleman, 1985; Curtis and Coleman, 1986; Hemibrook and Longstaffe, 1996; Mackay and Longstaffe, 1997; Morad, 1998; Rossi et al., 2001, for example). Moreover, siderite precipitation requires very low pO_2, very high pCO_2, a slightly acid to near neutral pH, and high concentrations of

Fig. 7. (a) Carbonate soil profile
(white arrows). (b) Detail of the carbonate nodules developed in the lower part of the Alcotas Formation. The pen for scale is 14 cm long. (c) Photomicrograph of a paleosol of the lower part of the Talayuelas section. Note nodulized dolomicrite (D) to the right, and the cracking structure, now replaced by coarse dolomite (CD), to the left. (d) Calcareous horizon of a soil profile
The pen for scale is 14 cm long. (e) Goethite replacing siderite aggregates developed in paleosols of the middle part of the Landete section. Note the presence of abundant lenticular pseudomorphs of siderite (arrows). The cap of the pen for scale is 3 cm long. (f) Backscattered SEM imagine of a siderite pseudomorphs aggregate. Note that goethite (G) preserves the external morphology of the siderite precursor. Ankerite (A) subsequently precipitated in the inner and outer part of the pseudomorphs and in fractures that affect aggregates (yellow arrow). (g) Backscattered SEM images of a siderite pseudomorph. Note that goethite (G) preserves the external morphology of the crystal and mimics the original cleavage of the siderite precursor. Ankerite (A) and calcite (C) subsequently precipitated in the inner and outer part of the pseudomorph. (h) Aspect of the upper part of the Alcotas Formation. The red beds (right of the photograph) are overlain by sandstone and carbonaceous shale (left). The scale bar is 15 cm long.

dissolved Fe^{2+} (Ohmoto et al., 2004). In contrast, pedogenic dolomite commonly occurs in well-aerated soils, and its precipitation requires relatively low pCO_2 (Wright and Tucker, 1991), and higher pH (Krumbein and Garrels, 1952) and Mg+Ca/Fe ratios (Coleman, 1985; Curtis and Coleman, 1986) than siderite precipitation. Thus, the environmental conditions likely changed towards more humid and acid during formation of siderite beds, which precipitated in poorly aerated and poorly drained areas. These environmental conditions agree with the presence of the carbonaceous shales and coal beds in the base of the upper part of the Landete section, and the type of plant remains of these levels that indicate a change towards more humid conditions (Diéguez and Barron, 2005).

Siderite is largely or completely replaced by goethite that precipitates under oxidizing conditions when siderite becomes unstable. Goethite is postdated by ankerite and calcite that precipitated during later stages of diagenesis (Fig. 7f, g). Thus, a recent replacement of siderite can be ruled out. It is also unlikely that goethite precipitated during burial of the unit but before ankerite and calcite precipitation, because burial diagenesis is dominated by reducing waters, and goethite typically precipitates under oxidizing humid, and acid conditions (Landon, 1991; Benison and Goldstein, 2002; Boul, 2003; Ohmoto et al., 2004; Tabor et al., 2004). Thus, it is probable that goethite precipitated during early stages of the diagenesis, before or soon after burial of paleosols. This is also supported by the presence of goethite accumulations in the Talayuelas section that preserve the original structure of plant remains, because iron-replacement of plant organic matter can occur on the order of weeks or years (Dunn et al., 1997; Tabor et al., 2004).

In the uppermost part of the Alcotas Formation, the lack of carbonate paleosols and plant remains would indicate a further step towards acid and oxidizing conditions. Such conditions have been broadly described for the end of Permian times (Erwin, 1993). This situation would continue until the Early Triassic, as indicated by the presence of Sr-rich aluminium sulphate phosphates (APS minerals) at the base of the Cañizar Formation. The formation of APS minerals is usually related to low pH environments (Spötl, 1992; Dill et al., 1995; Dill, 2001). In addition to the occurrence of APS minerals, the lack of carbonates and the widespread presence of hematite-rich red beds are features that may be considered as indirect evidence of an ancient acid system according to the criteria proposed by Benison and Goldstein (2002).

6. Concluding remarks

Three parts have been differentiated in the Late Permian continental sediments (Alcotas Formation) in SE Iberian Ranges (Spain) based on mineralogical and petrolelogical data and analysis of soil profiles. These parts can be related to changes in the palaeoenvironmental conditions.

The lower part would developed in an arid to semiarid climate with marked seasonality. Some evidences for these conditions include the presence of paleosols with shallow calcic horizons and the preservation of dolomicrite in some of the nodules.

In the middle part, a change in the palaeoenvironmental conditions can be recognized. Firstly, the presence of siderite in the paleosols and the occurrence of carbonaceous shales point to more humid and acid conditions in poorly areated and poorly drained areas. Secondly, these conditions evolved to more acid and oxidizing, as revealed by the presence of goethite both replacing siderite and as a former precipitate around plant remains towards the top of this middle part.

The upper part of the Alcotas Formation and the lower part of the Cañizar Formation would represent a further step towards acid conditions as indicated by the lack of carbonate paleosols and plant remains. The occurrence of APS minerals at the base of the latter unit would indicate extreme acid conditions.

Acknowledgments

The authors thank Modesto Escudero for drafting support, Gilberto Herrero and Beatriz Moral for thin section preparation, and Maribel Sevillano and Belén Soutullo for the assistance during XRD study. The staff of the Centro de Microscopía Luis Bru (Universidad Complutense, Madrid) is also acknowledged for the technical support during

the SEM and EPMA study. This work was financed by Project PTB2002-00775.

References

Alonso-Azcárate, J., Arche, A., Barrenechea, J.F., López-Gómez, J., Luque, F.J., Rodas, M., 1997. Palaeogeographical significance of clay mineral assemblages in the Permian and Triassic sediments of the SE Iberian Ranges, eastern Spain. Palaeogeogr. Palaeoclimatol. Palaeoecol. 136 (1–4), 309–330.

Alonso-Zarza, A.M., 2003. Palaeoenvironmental significance palustrine carbonates and calcretes in the geological record. Earth-Sci. Rev. 60, 261–298.

Arche, A., López-Gómez, J., 1996. Origin of the Permian–Triassic Iberian Basin, central-eastern Spain. Tectonophysics 266, 443–464.

Arche, A., López-Gómez, J., 1999. Tectonic and geomorphic controls on the fluvial styles of the Eslida Formation, Middle Triassic, Eastern Spain. Tectonophysics 315, 187–207.

Beauchamp, B., Baud, A., 2002. Growth and demise of Permian biogenic chert along northwest Pangea: evidence for end-Permian collapse of thermohaline circulation. Palaeogeogr. Palaeoclimatol. Palaeoecol. 184, 37–63.

Benison, K.C., Goldstein, R.H., 2002. Recognizing acid lakes and groundwaters in the rock record. Sediment. Geol. 151, 177–185.

Benton, M.J., 2003. When Life Nearly Died. The Greatest Mass Extinction of all Time. Thames & Hudson, London. 336 pp.

Boul, S.W., 2003. Soil Genesis and Classification. Ames, Iowa, USA. 494 pp.

Coleman, M.L., 1985. Geochemistry of diagenetic non-silicate minerals: kinetic considerations. Philos. Trans. R. Soc. Lond., A 315, 39–56.

Curtis, C.D., Coleman, M.L., 1986. Controls on the precipitation of early diagenetic calcite, dolomite y siderite concretions in complex depositional sequences. In: Gautier, D.L. (Ed.), Roles of Organic Matter in Sediment Diagenesis, SPEM Special Publication, vol. 38, pp. 23–34.

Dickson, J.A.D, 1966. Carbonate identification revealed by staining. J. Sediment. Petrol. 36, 491–505.

Diéguez, C., Barron, E., 2005. Upper Permian floral vegetation changes near the P/T boundary in the Landete section of the Alcotas Formation (SE Iberian Ranges, Spain). Palaeogeogr. Palaeoclimatol. Palaeoecol. 229, 54–68 (this issue).

Dill, H.G., 2001. The geology of aluminium phosphates and sulphates of the alunite group minerals: a review. Earth-Sci. Rev. 53, 35–93.

Dill, H.G., Fricke, A., Henning, K.-H., 1995. The origin of Ba- and REE-bearing aluminum-phosphate-sulphate minerals from the Lohreim kaolinitic clay deposit (Rheinisches Schiefergebirge, Germany). Appl. Clay Sci. 10, 231–245.

Doblas, M., Oyarzun, R., Sopeña, A., López-Ruiz, J., Capote, R., Hernández, R., Hoyos, J.L., Lunar, R., 1993. Variscan–Late Variscan–early Alpine progressive extensional collapse of Spain. Geodin. Acta 7, 1–14.

Doubinger, J., López-Gómez, J., Arche, A., 1990. Pollen and spores from the Permian and Triassic sediments of the southeastern Iberian Ranges, Cueva de Hierro (Cuenca) to Chelva–Manzanera (Valencia–Teruel) region, Spain. Rev. Palaeobot. Palynol. 66, 25–45.

Dunn, K.A., McLean, R.J.C., Upchurch Jr., G.R., Folk, R.L., 1997. Enhancement of leaf fossilization potential by bacterial biofilms. Geology 25, 1099–1122.

Erwin, D.H., 1993. The Great Paleozoic Crisis. Life and Death in the Permian. Columbia University Press, New York. 327 pp.

Erwin, D.H., 1996. Permian global bio-events. In: Wallister, O.H. (Ed.), Global Events and Events Stratigraphy in the Phanerozoic, pp. 251–264.

Fisher, M.J., Jeans, C.V., 1982. Clay mineral stratigraphy in the Permo-Triassic red bed sequences of BNOC 72/10-1A, Western Approaches, and the South Devon Coast. Clay Miner. 17, 79–89.

Gómez, J.J., Goy, A., 1999. Las unidades carbonatadas y evaporíticas del tránsito Triásico-Jurásico en la región de Lécera (Zaragoza, España). Cuad. Geol. Iber. 25, 13–23.

Hernando, S., Schott, J.-J., Thuigat, R., Montigny, R., 1980. Age des andesites et des sediments interstratifies d'Atienza (Espagne): Etude stratigraphyque et paleomagnetique. Sci. Geol., Bull. 33, 119–128.

Holster, W.T., Magaritz, M., 1992. Cretaceous/Tertiary and Permian/Triassic boundary events compared. Geochim. Cosmochim. Acta 56, 3297–3309.

Hornibrook, E.R.C., Longstaffe, F.J., 1996. Berthierine from the lower cretaceous clearwater formation, Alberta, Canada. Clay Clay Miner. 44, 1–21.

Jeans, C.V., Mitchell, J.G., Scherrer, M., Fisher, M.J., 1994. Origin of the Permo-Triassic clay mica assemblage. Clay Miner. 29, 575–589.

Jin, Y.G., Wang, Y., Wang, W., Shang, Q.H., Cao, C.Q., Erwin, D.H., 2000. Pattern of marine mass extinction near the Permian–Triassic boundary in south China. Science 289, 432–436.

Kozur, H.W., 1998. Some aspects of the Permian–Triassic boundary (PTB) and of the possible causes for the biotic crisis around this boundary. Palaeogeogr. Palaeoclimatol. Palaeoecol. 143, 227–272.

Krull, S.J., Retallack, G.J., 2000. $\delta^{13}C_{org}$ chemostratigraphy of the Permian–Triassic boundary in the Maitai Group, New Zeland: evidence for high-latitudinal methane release, New Zealand. J. Geol. Geophys. 43, 21–32.

Krumbein, W.C., Garrels, R.M., 1952. Origin and classification of chemical sediments in terms of pH and oxidation–reduction potentials. J. Geol. 60, 1–33.

Lago, M., Gil, A., Pocovi, A., Arranz, E., Galé, C., 2001. The Permian calc-alcaline magmatism of the Iberian Belt, Spain: an updated synthesis. Nat. Brescia. 25, 181–187.

Lago, M., Arranz, E., Pocovi, A., Galé, G., Gil-Imaz, A., in press. Permian magmatism of the Iberian Chain, Central Spain and its relationship with extensional tectonics. Spec. Publ. Geol. Soc. London 224.

Landon, J.R., 1991. Booker Tropical Soil Manual: A Handbook for Soil Survey and Agricultural Land Evaluation in the Tropics and

Subtropics. Longman Scientific & Technical, Harlow, England. 474 pp.

Lindgreen, H., Surlyk, F., 2000. Upper Permian–Lower Cretaceous mineralogy of East Greenland: provenance, palaeoclimate and volcanicity. Clay Miner. 35, 791–806.

Lippmann, F., Berthold, C., 1992. Der Mineralbestand des Unteren Muschelkalkes von Geislingen bei Schwäbisch Hall (Deutschland). Neues Jahrb. Mineral. Abh. 164, 183–209.

López-Gómez, J., Arche, A., 1993. Sequence stratigraphy analysis and paleogeographic interpretation of the Buntsandstein and Muschelkalk facies (Permo-Triassic) in the SE Iberian Ranges, eastern Spain. Palaeogeogr. Palaeoclimatol. Palaeoecol. 103, 347–361.

López-Gómez, J., Arche, A., Calvet, F., Goy, A., 1998. Epicontinental marine carbonate sediments of the Middle and Upper Triassic in the westernmost part of the Tethys Sea, Iberian Peninsula. In: Bachmann, G.H. Lerche, I. (Eds.), Epicontinental Triassic, Zentralblatt für Geologie und Paläontologie (1), 9–10, 1033-1084.

López-Gómez, J., Arche, A., Marzo, M., Durand, M., 2005. Stratigraphical and palaeogeographical significance of the continental sedimentary transition across the Permian–Triassic boundary in Iberia. Palaeogeogr. Palaeoclimatol. Palaeoecol. 229, 3–23 (this issue).

Lucas, J., 1962. La transformation des minéraux argileux dans la sedimentation: Études sur les argiles du Trias. Mem. Serv. Carte Geol. Alsace Lorraine 23 (202 pp.).

Machette, M.N., 1985. Calcic soils of southwestern United Stated. In: Weide, D.L. (Ed.), Soil and Quaternary Geology of the Southwestern United States, Special Paper, Geol. Soc. Amer., vol. 203, pp. 1–21.

Mackay, J.L., Longstaffe, F.J., 1997. Diagenesis of the lower cretaceous clearwater formation, Primrose Area, Northeastern Alberta. In: Pemberton, S.G., James, D.P. (Eds.), Petroleum Geology of the Cretaceous Mannville Group, Western Canada, Memoir, vol. 18. Canadian Society of Petroleum Geologists, pp. 392–412.

Marfil, R., Bonhomme, M.G., de la Peña, J.A., Penha dos Santos, R., Sell, I., 1996. La edad de las ilitas en areniscas Pérmicas y Triásicas de la Cordillera Ibérica mediante el método K/Ar; implicaciones en la historia diagenética y evolución de la cuenca. Cuad. Geol. Ibér. 20, 61–83.

Maxwell, W.D., 1992. Permian and Early Triassic extinction of non-marine tetrapods. Palaeontology 35, 571–584.

Menning, M., 2001. A Permian time scale 2000 and correlation of marine and continental sequences using the Illawarra reversal (265 MA). Nat. Brescia. 25, 355–362.

Morad, S., 1998. Carbonate cementation in sandstones: distribution patterns and geochemical evolution. In: Morad, S. (Ed.), Carbonate Cementation in Sandstones: Distribution Patterns and Geochemical Evolution, IAS Spec. Publ., vol. 26, pp. 1–26.

Mozley, P.S., 1989. Relation between depositional environment and the elemental composition of early diagenetic siderite. Geology 17, 704–706.

Muñoz, J.A., Casas, A.M., 1997. The Rioja trough: tectosedimentary evolution of a foreland symmetric basin. Basin Res. 9, 65–85.

Ohmoto, H., Watanabe, Y., Kumazawa, K., 2004. Evidence from massive siderite beds for a CO_2-rich atmosphere before ~1.8 billion years ago. Nature 429, 395–399.

Ortí, F., 1987. Aspectos sedimentológicos de las evaporitas del Triásico y del Liásico inferior en el E de la Península Ibérica. Cuad. Geol. Ibér. 11, 873–858.

Ortí, F., García-Veigas, J., Rosell, J., Jurado, M., Utrilla, R., 1996. Formaciones salinas de las cuencas triásicas de la Península Ibérica: caracterización petrológica y geoquímica. Cuad. Geol. Ibér. 20, 13–356.

Pérez-Arlucea, M., Sopeña, A., 1985. Estratigrafía del Pérmico y Triásico en el sector central de la Rama Castellana de la Cordillera Ibérica (provincias de Guadalajara y Teruel). Estud. Geol. 41, 207–222.

Ramos, A., 1979. Estratigrafia y paleogeografía del Pérmico y Triásico al oeste de Molina de Aragón (Província de Guadalajara). Semin. Estratigr., Ser. Monogr. 6, 1–313.

Ramos, A., Sopeña, A., Pérez-Arlucea, M., 1986. Evolution of Buntsandstein fluvial sedimentation in Northwest Iberian Ranges (Spain). J. Sediment. Petrol. 56, 862–875.

Raup, D.M., 1979. Size of the Permo-Triassic bottleneck and its evolutionary implications. Science 206, 217–218.

Retallack, G.J., 1993. Classification of paleosols: discussion. Geol. Soc. Amer. Bull. 105, 1635–1637.

Retallack, G.J., 1997. A Colour Guide to Paleosols. Wiley, Chichester, England. 175 pp.

Retallack, G.J., 1999. Postapocalyptic greenhouse paleoclimate revealed by earliest Triassic paleosols in the Sydney Basin, Australia. Geol. Soc. Amer. Bull. 111, 52–70.

Rossi, C., Marfil, R., Ramseyer, K., Permanyer, A., 2001. Facies-related diagenesis and multiphase siderite cementation and dissolution in the reservoir sandstones of the Khatatba Formation, Egypt's western desert. J. Sediment. Res. 71, 459–472.

Ruiz Cruz, M.D., 1996. Criterios mineralógicos empleados en el análisis del permotrías Maláguide. Cuad. Geol. Ibér. 20, 37–59.

Schultz, L.G., 1964. Quantitative interpretation of mineralogical composition from X-ray and chemical data from Pierce-Shale. Prof. Pap.-Geol. Surv. (U. S.) 391-C, C1–C31.

Sopeña, A., López-Gómez, J., Arche, A., Pérez-Arlucea, M., Ramos, A., Virgili, C., Hernando, S., 1988. Permian and Triassic rift basins of the Iberian Peninsula. In: Manspeizer, W. (Ed.), Triassic–Jurassic Rifting—Continental Breakup and the Origin of the Atlantic Ocean and Passive Margins, Developments in Geotectonics, vol. 22B. Elsevier, Amsterdam, pp. 757–786.

Sopeña, A., Doubinger, J., Ramos, A., Pérez-Arlucea, M., 1995. Palynologie du Permian et du Trias dans le Centre de la Péninsule Ibérique. Sci. Geol., Bull. 48, 119–157.

Spötl, C., 1992. Authigenic aluminium phosphate sulphates in sandstones of the Mitterberg Formation, Northern Calcareous Alps, Austria. Sedimentology 37, 837–845.

Spötl, C., Burns, S.J., 1994. Magnesite diagenesis in redbeds: a case study from the Permian of the Northern Calcareous Alps (Tyrol, Austria). Sedimentology 41, 543–565.

Spötl, C., Wright, VP., 1992. Groundwater dolocretes from the Upper Triassic of the Paris Basin, France: a case study of an arid, continental diagenetic facies. Sedimentology 39, 1119–1136.

Stanley, S.M., Yang, X., 1994. A double mass extinction at the end of the Paleozoic Era. Science 266, 1340–1344.

Tabor, N.J., Yapp, C.J., Montañez, I., 2004. Goethite, calcite, and organic matter from Permian and Triassic soils: carbon isotopes and CO_2 concentrations. Geochim. Cosmochim. Acta 68, 1503–1517.

Vargas, H., 2002. Análisis y comparación de la subsidencia entre las cuencas Ibérica y Ebro Central durante el Pérmico y el Triásico y su relación con el relleno sedimentario. PhD thesis. Universidad Complutense, Madrid, 310 pp. Unpublished.

Van Wees, J.D., Arche, A., Beijdorff, C., López-Gómez, J., Cloetingh, S., 1998. Temporal and spatial variations in tectonic subsidence in the Iberian Basin (eastern Spain): inferences from automated forward modelling of high-resolution stratigraphy (Permian–Mesozoic). Tectonophysics 300, 285–310.

Warr, L.N., Rice, H.N., 1994. Interlaboratory standardization and calibration of clay mineral crystallinity and crystallite size data. J. Metamorph. Geol. 12, 141–152.

Wignall, P.B., Morante, R., Newton, R., 1998. The Permo-Triassic transition in Spitsbergen: Corg. chemostratigraphy, Fe and S geochemistry, facies, fauna and trace fossils. Geol. Mag. 135 (1), 47–62.

Wright, V.P., Tucker, M.E., 1991. Calcretes: an introduction. In: Wright, V.P., Tucker, M.E. (Eds.), Calcretes, IAS Reprint Series, vol. 2. Blackwell, Oxford, pp. 1–22.

Ziegler, P.A., 1990. Geological atlas of western and Central Europe. Shell Internationale Petroleum Maastschappij BV. Int. Lithosphere Program 148, 1–239.

Ziegler, P., Stampfli, G.M., 2001. Late Paleozoic–Early Mesozoic plate boundary reorganization: collapse of the Variscan Orogen and opening of the Neotethys. Nat. Brescia. 25, 17–34.